Diversity in liquid supercooling and glass formation phenomena illustrated by a simple model

Daniela Kohen* and Frank H. Stillinger
Bell Laboratories, Lucent Technologies Inc., 600 Mountain Avenue, Murray Hill, New Jersey 07974
(Received 12 October 1998)

The opportunity to map condensed-phase inherent structures (potential energy minima) approximately onto the vertices of a high-dimensional hypercube provides simple conceptual and numerical modeling for first-order melting-freezing transitions, as well as for liquid supercooling and glass formation phenomena. That approach is illustrated here by examination of three interaction examples that were selected to demonstrate the diversity of thermodynamic behavior possible within this hypercube modeling technique. Two of the cases behave, respectively, as ''strong'' and ''fragile'' glass formers, at least as judged by their heat capacities. The third presents a ''degenerate glass,'' wherein full equilibration of the supercooling liquid (i.e., no kinetic arrest) leads to (a) residual entropy in the limit of absolute zero temperature, and (b) a linear temperature dependence of heat capacity in the same limit. None of the three cases displays a positive-temperature ideal (intrinsic) glass transition.

PACS number(s): 64.60.My, 05.90.+m, 61.90.+d, 82.20.Wt

I. INTRODUCTION

Substances that readily supercool as liquids below their equilibrium melting temperatures, and rigidify to form glasses upon further cooling, constitute a chemically very broad group [1,2]. As a result, their physical properties, both static and dynamic, present a wide range of behaviors [3]. This diversity continues to generate challenges to basic research on glass-forming materials, while at the same time offering many opportunities for technological application [4–6].

Because so many different molecular structures and interactions can be involved, it is difficult to construct a purely theoretical explanation of supercooling and glass formation that is both universally applicable and quantitatively predictive. Nevertheless, it is reasonable to expect that some theoretical approaches and/or models might attain some limited insights [3]. The present work is offered in this latter spirit; it is devoted to the further development of a previously introduced ''hypercube'' model [7,8] to show that it is capable of imaging glass diversity while raising some other conceptual issues.

On the phenomenological side, Angell has advocated a particularly useful classification scheme for glass-forming substances that arrays them between ''strong'' and ''fragile'' extremes [9]. The initial distinguishing feature in this scheme is the curvature of the Arrhenius plot of the logarithm of shear viscosity versus inverse temperature: the strong extreme shows none, the fragile extreme shows a substantial amount. The heat capacity behavior could as well have been used for the same classification, since strong materials (such as SiO_2) display virtually no change in heat capacity upon cooling through the glass transition temperature, while fragile materials (such as ortho-terphenyl) present a sudden large drop in heat capacity as the temperature declines through the narrow glass transition region [10].

Brief presentations of motivation and implementation for the hypercube model have appeared previously [7,8], but the following Sec. II revisits that background in a somewhat different form, for clarity and completeness. Section III introduces three alternative choices for interactions that operate in the model, chosen to illustrate strong, fragile, and ''degenerate glass'' behavior, respectively. The last of these is not usually considered in discussions of glass properties, but its low-temperature residual entropy and *classical* linear heat capacity merit examination. Section IV presents detailed numerical results for each of the three cases. Section V offers some conclusions and raises some general issues that deserve further study in the future.

II. HYPERCUBE MAPPING

The present study focuses on the mechanically stable configurations of the particles (atoms, ions, molecules) in a dense glass-forming substance. These are local minima of the potential energy function that comprises all interactions in the many-particle system, and have been called ''inherent structures'' [11–14]. These distinguished configurations form a discrete set; any other configuration can be resolved into an inherent structure and an intrabasin vibrational distortion [15,16]. An important technical point to bear in mind is that the potential energy function and its inherent structures depend upon whether constant volume or constant pressure conditions apply [17].

Suppose the glass-forming system of interest contains ν particle species, present respectively in numbers $N_1,\ldots,N_\nu$. Any one inherent structure is substantially equivalent to many others that differ only by permutation of positions of identical particles. It has been established [18] that under constant pressure or constant number density conditions, the large-system-limit behavior of the total number of inherent structures, Ω, exhibits the following asymptotic form:

*Present address: Department of Chemistry, University of California at Irvine, Irvine, CA 92717.

$$\ln\Omega \sim \alpha N + \sum_{j=1}^{\nu} \ln(N_j!), \tag{2.1}$$

where

$$\alpha > 0, \qquad N = \sum_{j=1}^{\nu} N_j . \tag{2.2}$$

The quantity α concerns the exponential rise rate, with increasing system size, of the number of distinguishable (i.e., unrelated by permutation) inherent structures; it can be expected to vary among substances, and to depend on pressure or number density.

Temperature dependence of the occupation probabilities for the various inherent structure basins constitutes a basic feature of liquid supercooling and glass formation. Postulating an approximate isomorphism between the $\exp(\alpha N)$ distinguishable inherent structures and the vertices of a D-dimensional hypercube offers a simplifying first step in understanding that temperature dependence. The number of hypercube vertices, 2^D, must equal the number of distinguishable inherent structures, so

$$D = (\alpha/\ln 2)N. \tag{2.3}$$

Thus the hypercube dimension scales linearly with N, as does the dimension of the original configuration space for the N-particle system.

Euclidean coordinate locations for hypercube vertices will be assigned by the following unit vectors [7,8].

$$\tau = D^{-1/2}(\pm 1, \pm 1, \pm 1, \ldots, \pm 1). \tag{2.4}$$

Each vertex has exactly D first neighbors whose locations differ by sign change of just one of the D entries in expression (2.4). The distance between first neighbors is $2D^{-1/2}$. More generally, each vertex has

$$\frac{D!}{n!(D-n)!} \tag{2.5}$$

nth neighbors $(1 \leqslant n \leqslant D)$, all at distance

$$2(n/D)^{1/2}. \tag{2.6}$$

The approximate isomorphism envisaged is not unique. Ideally, pairs of inherent structure configurations that are close in the original configuration space should map onto pairs of neighboring hypercube vertices. In particular, basins in the original space that share a common boundary should, to the extent possible, map onto nearest neighbor vertices. Typically, basins will contact on the order of N other basins, and on account of Eq. (2.3) the number of hypercube vertex nearest neighbors is also proportional to N, as required. It will be assumed in the following that the isomorphism has been selected so as to preserve these neighbor relationships in an optimal fashion. Among other attributes this implies that the potential energies of inherent structures that become nearest hypercube neighbors, although both $O(N)$ quantities, differ only by $O(1)$.

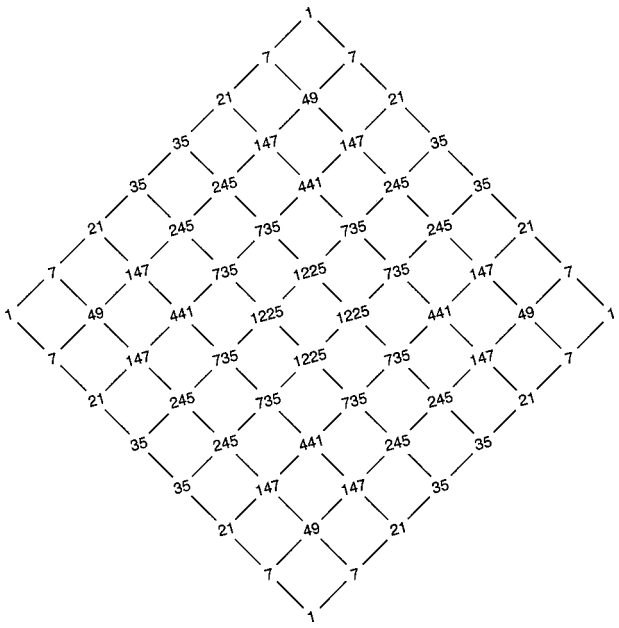

FIG. 1. Pattern of plane-projected vertex positions for the $D = 14$ hypercube. The integers shown at the $8^2 = 64$ positions are the respective degeneracies, the numbers of hypercube vertices that project to the same position.

Without incurring any significant loss of generality or error in the intensive quantities to be calculated below, it will be convenient to suppose that D is an even integer. Then it is possible to select a pair of unit vectors, $\boldsymbol{\tau}_x$ and $\boldsymbol{\tau}_y$, from the set (2.4) with the orthogonality property

$$\boldsymbol{\tau}_x \cdot \boldsymbol{\tau}_y = 0. \tag{2.7}$$

This merely requires that $D/2$ of the components of $\boldsymbol{\tau}_x$ and $\boldsymbol{\tau}_y$ agree, while the remaining $D/2$ components differ in sign. The entire collection of 2^D hypercube vertices can then be projected into the (x,y) plane defined by $\boldsymbol{\tau}_x$ and $\boldsymbol{\tau}_y$ with positions

$$x = \boldsymbol{\tau} \cdot \boldsymbol{\tau}_x, \qquad y = \boldsymbol{\tau} \cdot \boldsymbol{\tau}_y . \tag{2.8}$$

These plane-projected positions all fall on or within the square

$$|x+y| \leqslant 1, \qquad |x-y| \leqslant 1. \tag{2.9}$$

The pattern of projected vertex locations involves a regular array of $(D/2+1)^2$ points, far less than the total number of vertices when D (i.e., N) is large. Consequently, most of the locations host a large number of vertices. This characteristic is illustrated by Fig. 1, which explicitly displays the positions and multiplicities in the (x, y) plane for the specific case $D = 14$. Only the four hypercube vertices at $\pm\boldsymbol{\tau}_x$ and $\pm\boldsymbol{\tau}_y$ do not share positions [they are at the four corners of the square (2.9)].

In the large system limit, with N and D increasing to infinity, the set of projected positions becomes dense in square (2.9). As a result of simple combinatorial consider-

ations [7] it is straightforward to show that the multiplicity at position x,y has the asymptotic form $\exp[Dw(x,y)]$, where

$$w(x,y)=\ln 2-\tfrac{1}{4}[(1+x+y)\ln(1+x+y)+(1+x-y)\ln(1+x-y)+(1-x+y)\ln(1-x+y)+(1-x-y)\ln(1-x-y)]. \tag{2.10}$$

The selection of basis vectors $\boldsymbol{\tau}_x$ and $\boldsymbol{\tau}_y$ is not unique. The number of possibilities rises rapidly with increasing D. One can show that the number of distinct projection planes generated this way is given by the expression

$$\frac{2^{D-2}(D-1)!}{(D/2)!(D/2-1)!}. \tag{2.11}$$

This equals 7 028 736 for the modest $D=14$ example illustrated in Fig. 1.

III. HYPERCUBE INTERACTIONS

Calorimetric measurements on a wide variety of glass-forming substances indicate that the vibrational heat capacities of the crystal and of the amorphous glass states are approximately equal [10,19–21]. Vibrational degrees of freedom with high frequencies will manifest considerable quantum effects, especially at low temperature. But because these effects appear to be nearly identical in crystalline and amorphous phases, they can be dropped in calculation of the influence of temperature on inherent-structure basin occupation. This influence is the objective of the present class of hypercube models, for which classical statistical mechanics is now appropriate, and only the potential energies of the inherent structures themselves are relevant.

The large number of available plane projections, Eq. (2.11), offers a simplifying strategy. We choose that basis pair $\boldsymbol{\tau}_x,\boldsymbol{\tau}_y$ which comes closest statistically to having identical potential energies for all inherent structures that have a common projection location x,y. Then assuming that this requirement has been met to a satisfactory level of precision, the potential energy may be approximately expressed simply as

$$D\phi(x,y), \tag{3.1}$$

in other words as just a function of x and y. The factor D has been included to account for the fact that N-body potential energies are extensive quantities (i.e., proportional to N or equivalently to D), so that $\phi(x,y)$ is intensive.

The remaining two variables x and y should be regarded as measures of the amount and kind of disorder that is present in the many-particle system. Disorder in the crystalline state alone takes many forms, including vacancies, interstitials, orientational and conformational defects, dislocations, stacking faults, and grain boundaries. Liquid and amorphous solid states likewise must display disorder diversity. Consequently, it is reasonable to suppose that at least two ''disorder parameters'' are required to generate a unified description of crystalline and amorphous phases. At this crude level of description the crystalline solid on the one hand, and the liquid and glass on the other hand, could be expected to appear at distinct locations in the basic (x,y) square region (2.9), and indeed in the following Sec. IV this will be seen to occur.

An exploration of several reasonable forms for the potential energy function $\phi(x,y)$, in conjunction with the combinatorial entropy quantity $w(x,y)$, Eq. (2.10), shows that the hypercube model has the capacity to exhibit first-order melting, and a substantial variety of liquid supercooling behaviors. Two examples have been reported earlier [7,8], both of which could be classified as thermodynamically illustrating ''strong'' glass-former behavior. Three new cases will now be examined. These correspond respectively to the following three assignments, in suitable reduced energy units:

$$\phi_1(x,y)=x+y+0.6(x-y+0.05)^3-(x-y+0.05)^2-0.11/(x-y+1.11), \tag{3.2}$$

$$\phi_2(x,y)=3(x+y)+1.2(x-y+0.05)^3-(x-y+0.05)^2+0.15(x+y)(x-y+1)^4-0.11/(x-y+1.11), \tag{3.3}$$

$$\phi_3(x,y)=x+y+(x-y+0.1)^3-(x-y+0.1)^2-0.11/(x-y+1.11). \tag{3.4}$$

The ground state (lowest potential energy) for each of these cases occurs at the square vertex

$$x=-1,\qquad y=0. \tag{3.5}$$

Consequently, the ground state is nondegenerate, and corresponds to the structurally perfect crystal.

IV. NUMERICAL RESULTS

Let T^* stand for reduced temperature. The configurational free energy $F(T^*)$ for the hypercube model arises from the following minimization with respect to x and y over the square (2.9):

$$F(T^*)/DT^*=\min_{(x,y)}[\phi(x,y)/T^*-w(x,y)]. \tag{4.1}$$

Locating the position of the minimum, or minima, as T^* varies is a simple numerical task for each of the three cases defined above, Eqs. (3.2), (3.3), and (3.4). In the event that two (or more) local minima were to be found at some T^*, the one with the lower (or lowest) F of course would correspond to the thermodynamically stable phase, the other(s) to metastable phase(s).

Numerical analysis reveals that the three cases under present consideration share several qualitative attributes. Two local free energy minima exist at low T^*, the more stable one of which emerges from the vertex (3.5) as T^* increases above absolute zero. However, above a melting temperature T_m^* the other local minimum yields the lower free energy, and so can be identified as the ''liquid.'' The metastable ''crystal'' minimum persists above T_m^* until it

TABLE I. Properties calculated for the hypercube model with the three interaction choices.

Case	Strong	Fragile	Degenerate
T_m^*	6.686 2	7.697 0	7.014 8
T_c^*	8.642	10.042	9.232
$(\Delta w)_m$	0.344 07	0.301 03	0.343 82
$(C_{\rm liq}/C_{\rm cr})_m$	0.70	1.83	0.69
$\phi_g(T^*=0)$	−1.460 1	−5.165 5	−1.214 2
$w_g(T^*=0)$	0	0	0.267 8
$\phi_{\rm cr}(T^*=0)$	−3.416 9	−5.931 4	−3.539 0
$w_{\rm cr}(T^*=0)$	0	0	0

vanishes at a higher finite instability temperature T_c^*. For $T^*>T_c^*$ only the liquid minimum exists, and its location approaches $x=y=0$ as T^* approaches infinity. Table I collects the computed values of T_m^*, T_c^*, and several other quantities to be discussed below for each of the three interactions.

Figures 2, 3, and 4, show the paths traced by the free energy minima as temperature varies, for each of the three cases. The respective thermodynamic melting points are graphically identified by pairs of small open circles, between which the system discontinuously jumps upon passing the melting-freezing first-order phase transition. The crystal branch (cr) behaves similarly for all three cases, emanating from the $x=-1$, $y=0$ square vertex and moving diagonally upward nearly along a side of the square as T^* rises from zero. And in all three cases the liquid (liq) path is well separated in the square from that of the crystal, indicating clear structural distinctiveness for the two phases.

The liquid-phase paths for cases 1 (strong) and 2 (fragile), Figs. 2 and 3, respectively, are qualitatively similar though clearly differing in shape detail. Both begin at vertex $x=0$, $y=-1$ at $T^*=0$ as nondegenerate (zero entropy) glasses.

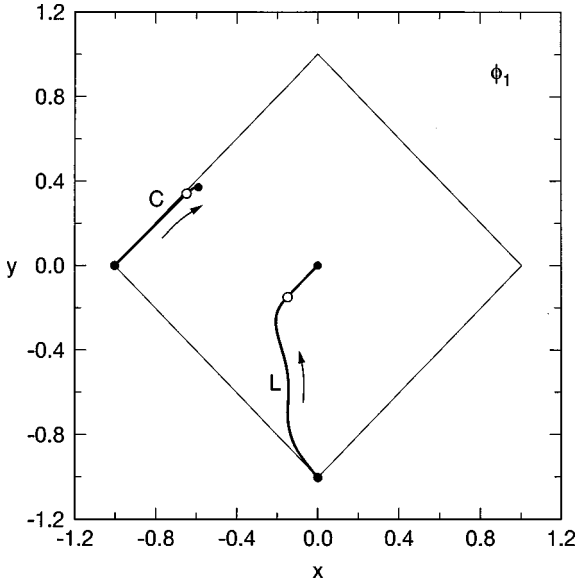

FIG. 2. Paths traced out in the (x,y) square for the crystal (cr) and liquid (liq) phases for interaction choice ϕ_1. The arrows indicate the direction of increasing temperature, and open circles locate T_m^*, the thermodynamic melting-freezing transition.

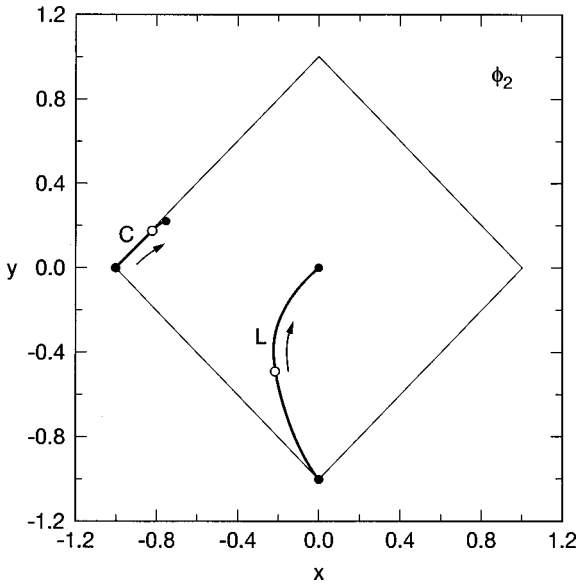

FIG. 3. Crystal and liquid paths in the (x,y) square for interaction choice ϕ_2. The notation is the same as that used in Fig. 2.

The potential energies of these ideal glass states, $\phi_g(T^*=0)$, along with the corresponding ideal crystal potential energies, $\phi_{\rm cr}(T^*=0)$, appear in Table I.

Case 3 presents a glass-state anomaly. Its zero temperature limit lies along a square edge, at position

$$x=-0.227\,017,$$
$$y=-0.772\,983. \tag{4.2}$$

Consequently, this state is configurationally degenerate. The extent of this degeneracy is measured by the value of w at the square-side position (4.2), and is listed in Table I as the quantity $w_g(T^*=0)$.

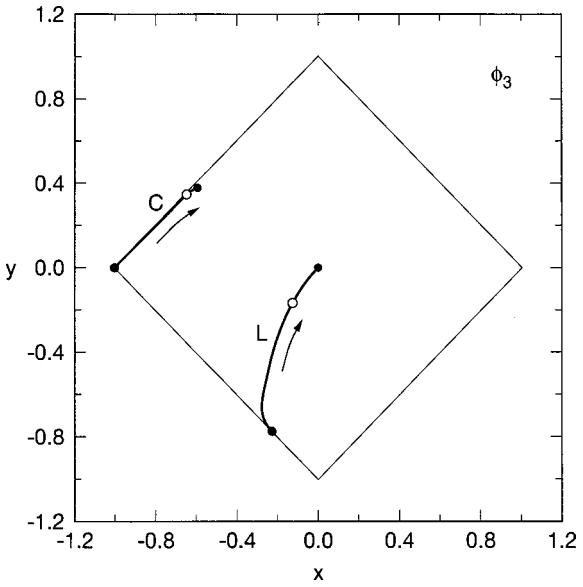

FIG. 4. Crystal and liquid paths in the (x,y) square for interaction choice ϕ_3. The notation is the same as that used in Figs. 2 and 3.

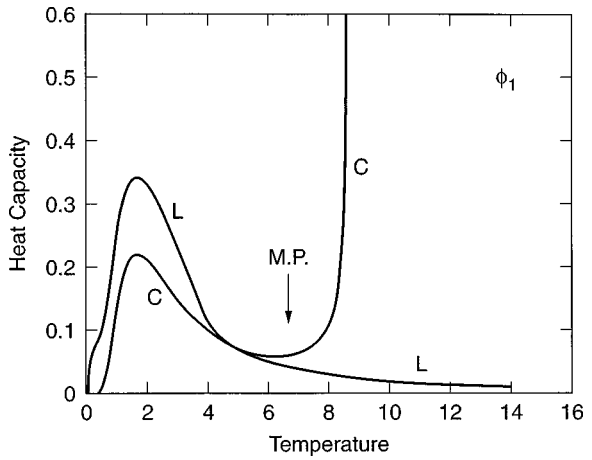

FIG. 5. Heat capacity curves for interaction choice ϕ_1. The arrow locates the equilibrium melting-freezing transition.

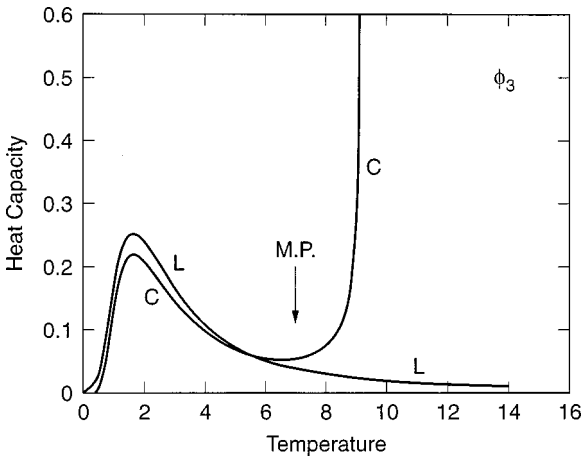

FIG. 7. Heat capacity curves for interaction choice ϕ_3. The arrow locates the equilibrium melting-freezing transition.

Figures 5, 6, and 7 show the curves for heat capacity $c = d\phi/dT^*$ calculated for the three cases, with distinct branches for the crystal and the liquid phases. As T^* approaches T_c^* from below, the crystal heat capacity for all three cases diverges to infinity (one can show that these are inverse-square-root singularities). The roughly comparable heat capacities for crystal and liquid in case 1 merit the classification ''strong,'' while the large difference between them in case 2 (particularly below T_m^*) justifies the label ''fragile.'' On this basis the ''degenerate'' case 3 (Fig. 7) would also be classified as strong.

All numerical results displayed in Figs. 2–7 assume that local equilibration in the (x,y) space for location of free energy minima is operative. In the case of real glass-forming substances this equilibration becomes kinetically arrested at and below a glass transition temperature T_g^*,

$$0 < T_g^* < T_m^*. \tag{4.3}$$

Kinetics of configurational transitions are an attribute of the hypercube models that is logically independent of the thermal features, and are therefore outside the scope of the present paper. However, the reader should keep in mind that a ''realistic'' glass transition would terminate a liquid-branch configurational heat capacity at T_g^*, which thereupon substantially vanishes at lower T^*. Analogously, one must realistically expect a superheated crystalline phase kinetically to melt well before reaching its instability temperature T_c^*.

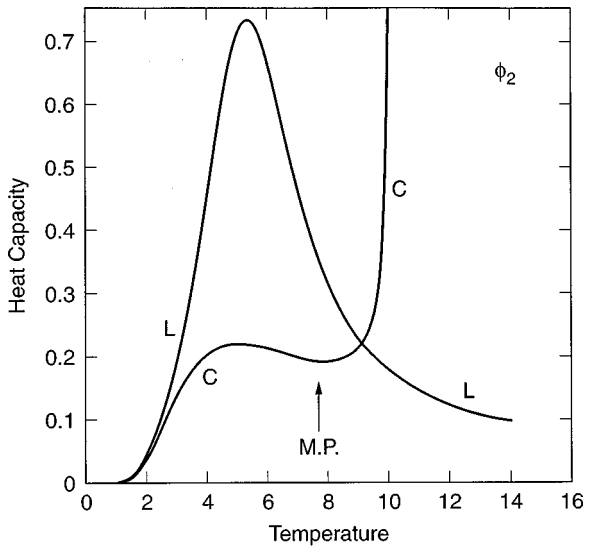

FIG. 6. Heat capacity curves for interaction choice ϕ_2. The arrow locates the equilibrium melting-freezing transition.

All three crystal heat capacity curves, and the liquid curves for cases 1 and 2, vanish exponentially as T^* approaches zero. Once again the ''degenerate'' case 3 is anomalous; its liquid-branch configurational heat capacity is linear in T^* in the low-temperature limit. By using low-order expansions for $w(x,y)$ and $\phi_3(x,y)$ in the vicinity of position (4.2), one can show

$$c_3(T^*) = 0.051\,34T^* + O(T^{*2}). \tag{4.4}$$

Such linear dependence is reminiscent of that observed in low-temperature amorphous solids, and associated with quantum mechanical two-level tunneling degrees of freedom [22,23]. However, the present example is quite different, arising as it does in a classical statistical mechanical setting. In view of the fact that a positive-temperature glass transition would preempt direct calorimetric observation of a linear heat capacity of type (4.4), it will be a substantial challenge to determine if any real substances fall into our ''degenerate'' glass category.

V. CONCLUSIONS AND DISCUSSION

The three interaction choices examined in this paper, Eqs. (3.2)–(3.4), supplementing the two cases previously studied [7,8], demonstrate that the hypercube model possesses considerable diversity in the thermodynamic behavior it can display. In particular, it is now clear that insofar as heat capacity is concerned, the model can span the full range between ''strong'' and ''fragile'' extremes by relatively simple alteration in the interaction function $\phi(x,y)$. This flexibility in behavior is sufficient in fact to have produced theoretically a third type of glass former, the ''degenerate'' type exemplified by $\phi_3(x,y)$, Eq. (3.4).

Some glass-forming substances exhibit crystal polymorphism. Silicon dioxide (SiO_2) is a well-known example

[24,25], with quartz, cristobalite, tridymite, coesite, and stishovite predominating in distinct temperature-pressure regimes. An adroit choice of interaction function $\phi(x,y)$ should allow the hypercube model also to possess two or more low-temperature ''crystal'' phases, each stable in some temperature interval below the melting point at T_m^*. For example, their individual paths in the fundamental (x,y) square could emanate from distinct vertices of the square as T^* increases from absolute zero.

The three examples studied in the present paper seem to be more realistic in at least one important respect than the examples that were presented in Refs. [7] and [8]. One can see from entries in Table I that the ratio T_c^*/T_m^* measuring the maximum possible extent of crystal superheating is close to 1.3 for each of the present cases. By contrast, the corresponding ratios in Refs. [7] and [8] were approximately 2.3 and 1.7, respectively. To stress a previous point, flexibility in choice of $\phi(x,y)$ beyond that already exercised should permit T_c^*/T_m^* to be reduced even further toward unity, should experimental observation so dictate.

One obvious, but benign, shortcoming of the hypercube model examples as thus far implemented concerns their behavior at the thermodynamic melting point T_m^*. This is a first-order phase transition that should permit, in principle, coexistence of the two phases in arbitrary relative amounts without changing the free energy (interfacial terms are insignificant in the present context that only concerns the large-system limit). This implies that at T_m^* some continuous path must exist in the (x,y) plane connecting the pure-phase locations (pairs of open circles in Figs. 2, 3, and 4) along which the free energy is invariant. Hypercube model cases examined thus far do not show this behavior, a shortcoming that can be patched up ''after the fact'' by redefining $\phi(x,y)$ appropriately within a domain that exists between (and is tangent to, at the T_m^* points) the phase paths already traced out. The correspondingly modified $\phi(x,y)$ should be continuous within the (x,y) square. This *a posteriori* procedure is analogous to the Maxwell double tangent construction [26] that identifies liquid-vapor coexistence regions for equations of state of the van der Waals type.

Equation (2.3) above presented the formal relation between the hypercube dimension D for a given number N of particles, and the parameter α that measures the number of distinct inherent structures. Recently, α has been estimated [27] for the fragile glass former prototype ortho-terphenyl (OTP), using accurate calorimetric data for that substance [10], with the result:

$$\alpha(\mathrm{OTP}) \cong 13.14. \tag{5.1}$$

Consequently, Eq. (2.3) requires

$$D/N \cong 18.96. \tag{5.2}$$

To the extent that the ''fragile'' case (ϕ_2) is a reasonable statistical model for OTP, this becomes its dimension assignment.

Historically, one of the prominent concepts in glass science concerns the second-order ''ideal glass transition'' at some positive temperature T_0^* less than the observed glass transition temperature [28]. This is the point hypothetically at which cooling of an equilibrated, supercooled liquid would attain substantially vanishing configurational entropy. The concept seems to be especially attractive for fragile glass formers (such as OTP) because of near coincidence between the calorimetric Kauzmann temperature and the apparent divergence temperature of shear viscosity and of mean structural relaxation time [3]. However, none of the hypercube models previously investigated [7,8] or examined in this paper exhibit a second-order ideal glass transition. Indeed, general counterarguments exist against such a possibility [29]. Nevertheless, it is legitimate to ask whether the hypercube model is capable *in principle* of producing a second-order ideal glass transition in its supercooled liquid phase, and if so what are the corresponding requirements on the interaction function $\phi(x,y)$. It is not appropriate to pursue this point in great detail here, but suffice it to say that such transitions can be produced if $\phi(x,y)$ has a bounded logarithmic singularity (of type $z \ln z$) located at the liquid-state square vertex.

Finally, kinetic properties of the hypercube model deserve mention in passing. One approach involves development of a Fokker-Planck equation in order-parameter (x,y) space [7], and its extension to incorporate time-lag phenomena [8]. These formalisms remain largely unexplored at present, and may be productive directions for future work.

[1] P. G. Debenedetti, *Metastable Liquids* (Princeton University Press, Princeton, NJ, 1996), Chap. 4.
[2] C. A. Angell, Science **267**, 1924 (1995).
[3] J. Jäckle, Rep. Prog. Phys. **49**, 171 (1986).
[4] R. H. Doremus, *Glass Science*, 2nd ed. (Wiley-Interscience, New York, 1994).
[5] J. Fricke, Sci. Am. **258**(5), 92 (1988).
[6] A. L. Greer, Science **267**, 1947 (1995).
[7] F. H. Stillinger, J. Phys. Chem. **88**, 6494 (1984).
[8] F. H. Stillinger, Physica D **107**, 383 (1997).
[9] C. A. Angell, J. Non-Cryst. Solids **131-133**, 13 (1991).
[10] S. S. Chang and A. B. Bestul, J. Chem. Phys. **56**, 503 (1972).
[11] H. Tanaka and K. Nakanishi, J. Chem. Phys. **95**, 3719 (1991).
[12] A. Z. Patashinski and M. A. Ratner, J. Chem. Phys. **106**, 7249 (1997).
[13] F. L. Somer, Jr., G. S. Canright, T. Kaplan, K. Chen, and M. Mosteller, Phys. Rev. Lett. **79**, 3431 (1997).
[14] D. S. Corti, P. G. Debenedetti, S. Sastry, and F. H. Stillinger, Phys. Rev. E **55**, 5522 (1997).
[15] F. H. Stillinger and T. A. Weber, J. Chem. Phys. **80**, 4434 (1984).
[16] F. H. Stillinger, Science **267**, 1935 (1995).
[17] F. H. Stillinger, Phys. Rev. B **41**, 2409 (1990).
[18] F. H. Stillinger, Phys. Rev. E **59**, 48 (1999).
[19] S. S. Chang, J. A. Horman, and A. B. Bestul, J. Res. Natl. Bur. Stand., Sect. A **71A**, 293 (1967).
[20] C. A. Angell and J. C. Tucker, J. Phys. Chem. **78**, 278 (1974).
[21] P. G. Debenedetti, *Metastable Liquids* (Ref. [1]), p. 244.
[22] W. A. Phillips, J. Low Temp. Phys. **7**, 351 (1972).
[23] P. W. Anderson, B. I. Halperin, and C. M. Varma, Philos.

Mag. **25**, 1 (1972).
[24] R. B. Sosman, *The Phases of Silica* (Rutgers University Press, New Brunswick, NJ, 1965).
[25] N. R. Keskar and J. R. Chelikowsky, Phys. Rev. B **46**, 1 (1992).
[26] K. Huang, *Statistical Mechanics* (Wiley, New York, 1963), p. 45.
[27] F. H. Stillinger, J. Phys. Chem. **102**, 2807 (1998).
[28] M. Goldstein, J. Chem. Phys. **67**, 2246 (1977).
[29] F. H. Stillinger, J. Chem. Phys. **88**, 7818 (1988).